

**A. Złocki, M. Roskosz\*, J. Kwaśniewski**

*AGH University of Science and Technology, Department of Machine Engineering and Transport, A. Mickiewicza st., 30-059 Krakow, Poland*

*\*mroskosz@agh.edu.pl*

## **THE INFLUENCE OF PULSATING TENSILE STRESS ON RESIDUAL MAGNETIC FIELD OF P91 STEEL SAMPLES**

### **ABSTRACT**

Measurements of Residual Magnetic Field RMF (the tangential component parallel to the load direction) were taken on the surface of P91 steel plate samples (X10CrMoVNb9-1) subjected to periodic pulsating tensile cyclic loads with the use of flux-gate and magnetoimpedance sensors, and preliminary measurement results are compiled and analyzed. The study investigates how the microstructure and load cycle parameters affect the RMF changes due to stress variations. Each combination of parameters: microstructure and load cycle corresponds to the characteristic variability pattern of magnetization and its maximum and minimum values.

**Keywords:** *P91 steel, residual magnetic field, magnetization, measurement, microstructure*

### **INTRODUCTION**

In the light of increasingly demanding requirements as to mechanical properties of materials for the power generation sector, there is a growing need of materials having sufficient resistance and yield strength at high temperatures. In terms of their performance of, the creep strength and thermal fatigue of these materials are equally important. Power steels are used in the production of steam turbines, boiler pipes, collectors and high-pressure pipelines, boiler fittings.

P91 boiler steel (X10CrMoVNb9-1) is increasingly used in the power industry for manufacturing of pipes, sheets, forgings and bars, replacing typical standard grades such as 13HMF and 14MoV6-3. It belongs to the group of high-alloy and high-temperature boiler steels because of the increased content of chromium and small amounts of less common alloy additives.

A growing number of increasingly sensitive magnetic field sensors enable the development of diagnostic methods based on the measurement of magnetic field strength on or near the surface of the investigated elements. The expertise in the use of magnetic field strength of RMF [1, 2], modern sensors and analysis of diagnostic signal [3, 4] alongside the unflagging interest in this research area [3 - 9] have prompted the analysis of feasibility of

using selected sensor types (flux-gate and magnetoimpedance sensors) for assessing the condition of ferromagnetic elements. Tests involved the measurement of the tangential component RMF(residual magnetic field) acting parallel to the direction of the applied load. Measurements were carried out on the surface of P91 steel specimens with different microstructure, subjected to periodic pulsating tensile cyclic loads. The purpose of the test was:

- Qualitative and quantitative comparison of readouts from various types of sensors,
- analysis of the influence of microstructure and the stress of the maximum cycle on RMF values.

## THEORETICAL BACKGROUNDS

On the macroscopic scale, mechanical and magnetic properties of ferromagnetics are interrelated. A ferromagnetic subjected to a magnetic field changes both its state of magnetization as well as dimensions. In turn, under the influence of mechanical stresses in the ferromagnetic, deformations arise accompanied by a change in magnetization. Magnetomechanical coupling can be formally expressed by a relationships in which the tensor of total strain  $\epsilon$  is the result of the simultaneous action of stresses  $\sigma$  causing the deformations  $\epsilon_\sigma$  and the magnetic field  $H$  causing the strain  $\epsilon_H$ . Similarly, induction  $B$  is the sum of  $B_\sigma$  induction resulting from stress and  $B_H$  induction resulting from the magnetic field  $H$ .

$$\begin{cases} \epsilon = \epsilon_\sigma + \epsilon_H = S\sigma + D^\sigma H \\ B = B_\sigma + B_H = D^H \sigma + \mu H \end{cases} \quad (1)$$

In the equations (1)  $D^\sigma = \frac{\partial \epsilon}{\partial H} \Big|_\sigma$ ,  $D^H = \frac{\partial B}{\partial \sigma} \Big|_H$  are magnetomechanical coefficients determined at constant stresses and a constant magnetic field,  $S$  is the compliance matrix [12 - 14].

The intensity of RMF near the ferromagnetic object can be derived from

$$H(r) = H_a(r) + H_d(r) \quad (2)$$

where  $H_a$  is intensity of the external magnetic field, and  $H_d$  is intensity of the magnetic field caused by magnetization of the ferromagnetic.  $H_d$  is called the demagnetization field and it is governed by

$$H_d(r) = \frac{1}{4\pi} \int_V \frac{-\nabla \cdot M(s)}{|r-s|^3} (r-s) dV(s) + \frac{1}{4\pi} \int_S \frac{n \cdot M(s)}{|r-s|^3} (r-s) dS(s) \quad (3)$$

where  $M$  - magnetization,  $V$  - volume,  $S$  - surface area of the ferromagnetic, and  $s$  - the vector for any inner point or on the surface of the magnetometer,  $r$ . The values and distribution of

magnetization  $M(s)$  give rise to a unique distribution and values of magnetic field strength  $H(r)$ .

## EXPERIMENTAL

The geometry of investigated samples in the form of P91 steel plates (X10CrMoVNb9-1) is shown in Figure 1 and their strength properties and chemical composition are given in Table 1. The samples were subjected to various heat treatment processes and thus produced microstructures are illustrated in Fig 2.

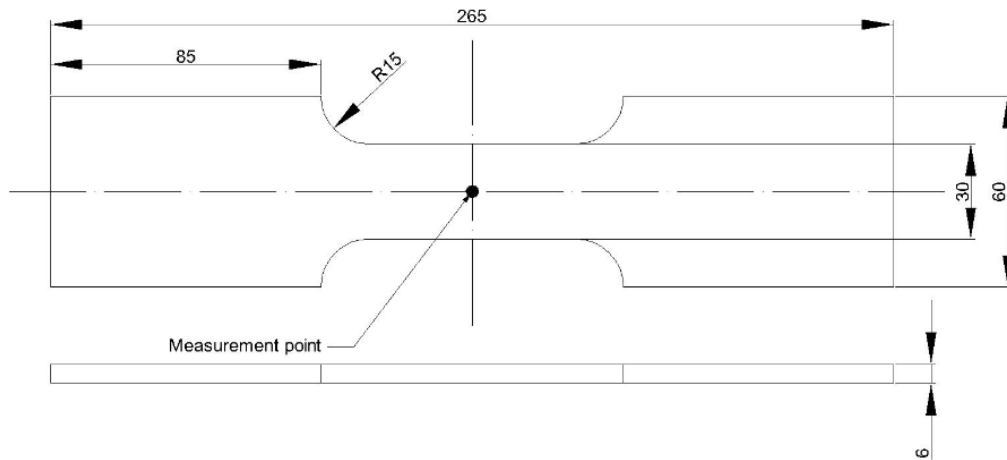
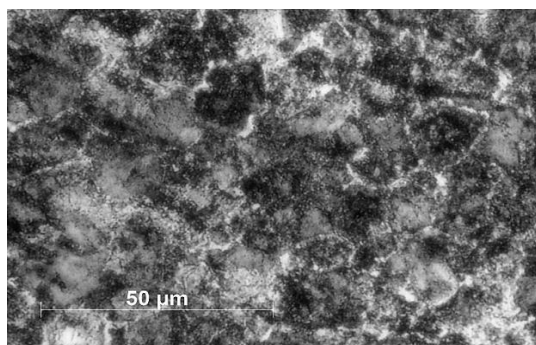


**Fig.1.** Geometry of the sample with the measuring point marked

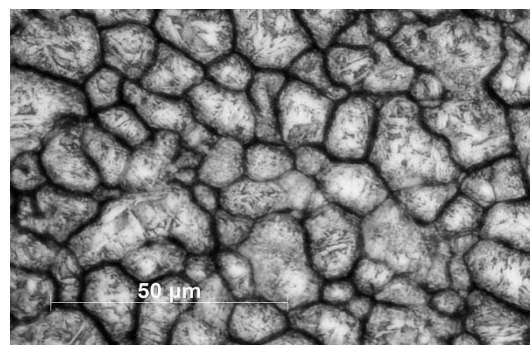
**Table 1.** Mechanical properties and chemical composition of P91 steel (X10CrMoVNb9-1)

Mechanical properties														
R <sub>e</sub> : > 435 MPa							R <sub>m</sub> : 550 – 760 MPa							
Chemical composition, wt.%														
C	Mn	Si	P	S	Cr	Ni	Mo	V	Nb	Ti	Al	N	Zr	Cu
0.08 - 0.12	0.3 - 0.6	0.2 - 0.5	<0.02	<0.005	8.0 - 9.5	<0.4	0.85 - 1.05	0.18 - 0.25	0.06 - 0.10	<0.01	<0.02	0.03 -0.07	<0.01	<0.3

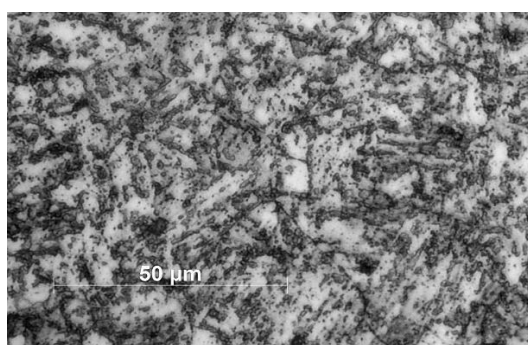
The basic stages of P91 steel manufacturing process include normalization at 1050-1060°C and then tempering at 750-760°C. As a result, in the material structure is modified, giving the desired mechanical properties.



The sample is normalized at 1060 °C (furnace, air), then cooled in the furnace - sample 1.  
Microstructure: fine ferrite grains with numerous fine coagulated carbides, also few fine ferrite grains without precipitates and ferrite areas along grain boundaries and their surroundings.



The sample after oil quenching from 1060 °C (furnace, air) and after tempering at 750 °C (furnace, air) - sample 2.  
Microstructure: martensite with a small amount of residual austenite and irregular fine ferrite areas with visible grain boundaries of primary austenite.



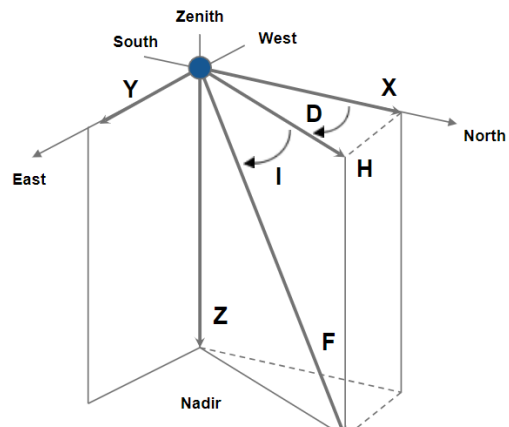
Sample in delivery condition - sample 3  
Microstructure: highly dispersed martensite with numerous coagulated fine carbides and few small irregular ferrite areas.  
Visible grain boundaries of primary austenite.

**Fig. 2.** Microstructures of the tested samples

Each sample was subjected to 30 cycles of pulsating tensile stress loads with a maximum load value inducing in a smaller sample cross-section the maximum stress of the cycle, 100, 200 and 400 MPa, respectively. The H100K-S HOUNSFIELD Materials Testing Machine [15] was used for load application. Load increase and unloading took place at the rate of 2 mm/min. Before the tests, the samples were demagnetized in the DZC100 coil, manufactured by the PTS Josef Solnar company[16]. This process was repeated before each increase in the maximum tensile force. The sample was compressed to obtain a zero elongation. A higher value of compressive force was required with each cycle run.

The expected distribution of the Earth's magnetic field without the influence of local magnetic anomalies in the laboratory was determined on the basis of the following model WMMv2\_2019 [19]. The input data included: latitude: 50°3'37''N, longitude: 19°55'56''E, altitude above sea level: 200m and date on which the measurements were taken. The expected field parameters are shown in the Table 2.

**Table 2.** Reference parameters of the Earth's magnetic field

Magnetic field components	Magnetic induction [nT]	Magnetic field strength [A/m]	
Horizontal	19830,6	15,81	
North Comp	19739,3	15,74	
East Comp	1900,9	1,51	
Vertical Comp	45406,2	36,22	

Two types of sensors were used in the measurement procedure: flux-gate and Mi sensors calibrated by two different methods before recording the magnetic field distribution in the vicinity of the tested sample. The first instrument as well as the sensors designated for RMF measurements were manufactured by "Energodiagnostika" [17], a company based in Moscow. The TSC-3M-12 (Tester of StressConcentration) magnetometer and a TSC-2M multichannel flux-gate sensor (fluxgatemagnetometer) allow the measurements of magnetic field strength in the range of  $\pm 2,000$  A/m, with an error of  $\pm 5\%$ , with sensitivity level 1 A/m). It enables manual surface scanning, automatic measurement and recording of measured fields. The second sensor used is SpinMeter3D manufactured by "Micro MagneticsSensible Solutions" [18] alongside the dedicated computer software for recording magnetic field readouts. The measuring range of the sensor is  $\pm 1000$   $\mu$ T, offering a sensitivity of  $0,1\mu\text{T} \approx 0,08$  A/m. Comparison of sensitivity features of the two sensors indicates that the MI sensor is tenfold more sensitive than the transducer sensor.

The flux-gate sensor was calibrated to handle magnetic field values of 40 A/m. After starting the device, the calibration option was selected, initially the calibration was performed in the sensor's x axis by setting the expected magnetic field at '40 A/m' (the anticipated vertical field components '36,22 A/m' – Table 2.) followed by the instructions displayed on the screen (to place the sensor in the upper position, then the lower position). The procedure was repeated for the y axis.

In the case of the SpinMeter3D sensor, a tube made of rolled metal alloy (Mu-Metal) of nickel, molybdenum and iron was used, which has high magnetic permeability thus ensuring a high level of damping. Magnetic field strength inside the tube was zero and the sensor was calibrated accordingly every time the program was started. Because the tube has no ending at one end, the calibration produces an intensity value around 0 A/m in each axis. In its measuring range, the sensor has a linear characteristic and the directional factor has been programmed in the sensor during the factory calibration.

Following the calibration of the sensors, the registered values of the magnetic field were duly compared. Measurement results were found to be similar and the difference registered for the undisturbed Earth's magnetic field did not exceed 2%. In the next step, the influence of the horizontal component of the Earth's field perpendicular to the surface of the specimen and the level of magnetic field disturbances generated by fatigue machine elements were

determined accordingly as these data are necessary for numerical correction of measurement results.

In the next step, two types of sensors were used to measure the magnetic field of the sample parallel to the applied tangential load. They were positioned on two sides of the sample placed in the cylinder head so as to measure the magnetic field in the middle section of the sample. The casings of both sensors were clutched to the surface of the samples, it follows that the sensor element of the MI sensor is located at a distance of 3mm from the surface of the sample, whilst the construction of the transducer sensor is such that the distance of the measuring element from the tested surface could not be precisely determined.

## MEASUREMENT RESULTS AND THEIR DISCUSSION

Measurement data would yield the time profiles of RMF values obtained for three components on the surface of the tested samples. According to literature reports, the largest component changes are those parallel to the applied load, tangent to the surface of the investigated sample [10-11]. These results were correlated with the stress changes and the halves of the magnetomechanical hysteresis loop were obtained accordingly. In Figures 3 to 6, the red color represents the readouts obtained while the load was being applied to the sample, and the blue color represents the load relief stage. It was assumed that the readouts from the magneto-impedance and flux-gate sensor obtained for the same sample will be presented side by side. A selected plot illustrating the stabilization process is a magnetoelastic hysteresis loop measured for sample 1 and the maximum stress within the loading cycle of 400 MPa is shown in Fig. 3a for the magneto-impedance sensor and for the flux-gate (Fig 3b)

Figures 4 to 6 show the magnetization curves measured for the test samples for the stabilized magneto-mechanical hysteresis loop.

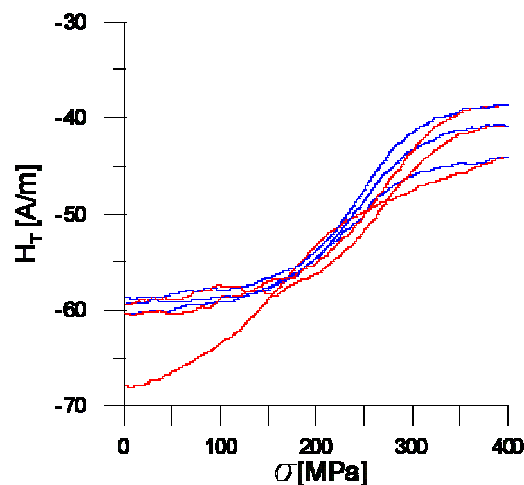


**Fig. 3a.** Magnetizing curves for the first three cycles at a maximum tension of 400 MPa for sample 1 - MI sensor

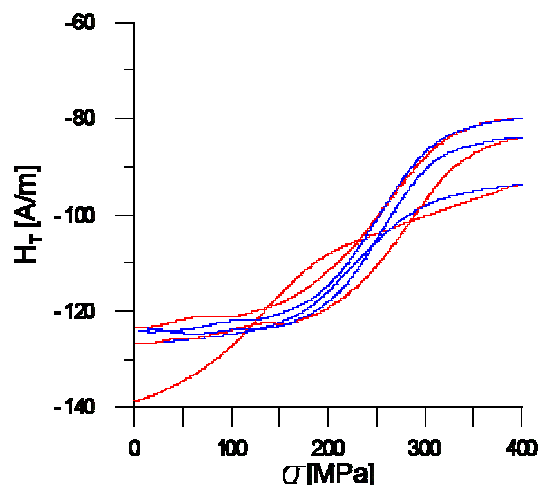


**Fig. 3b.** Magnetizing curves for the first three cycles at a maximum tension of 400 MPa for sample 1 - flux-gate sensor

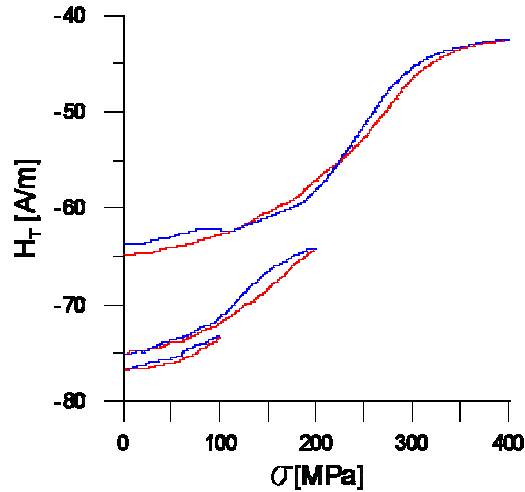


**Fig. 4a.** Magnetizing curves for a stabilized magneto-mechanical hysteresis loop - sample 1, MI sensor

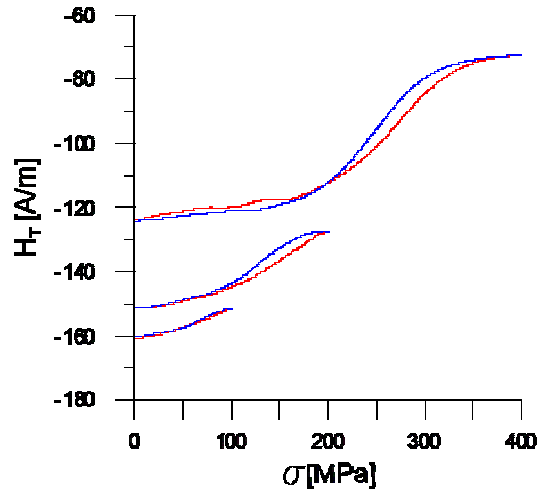


**Fig. 4b.** Magnetizing curves for a stabilized magneto-mechanical hysteresis loop - sample 1, flux-gate sensor

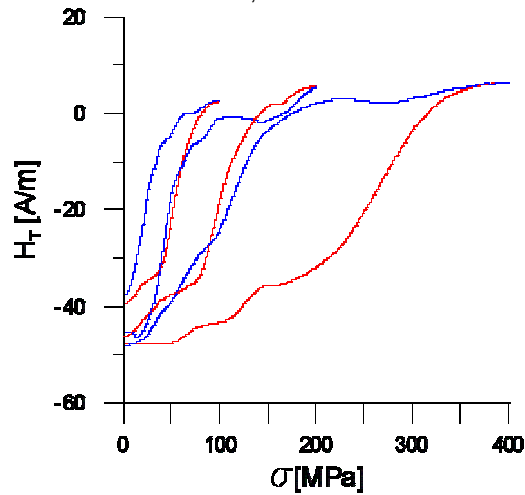


**Fig. 5a.** Magnetizing curves for a stabilized magneto-mechanical hysteresis loop test 2, MI sensor

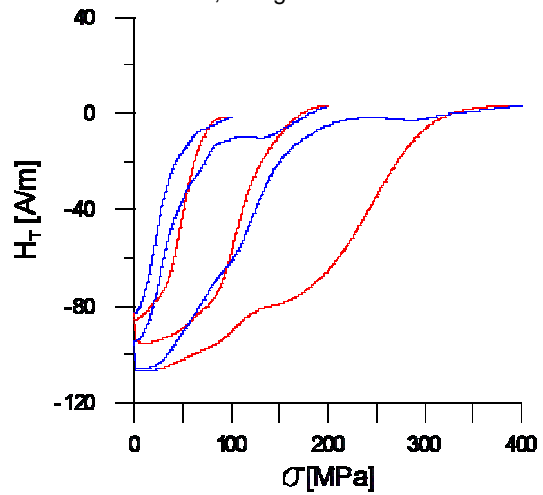


**Fig. 5b.** Magnetizing curves for a stabilized magneto-mechanical hysteresis loop test 2, flux-gate sensor

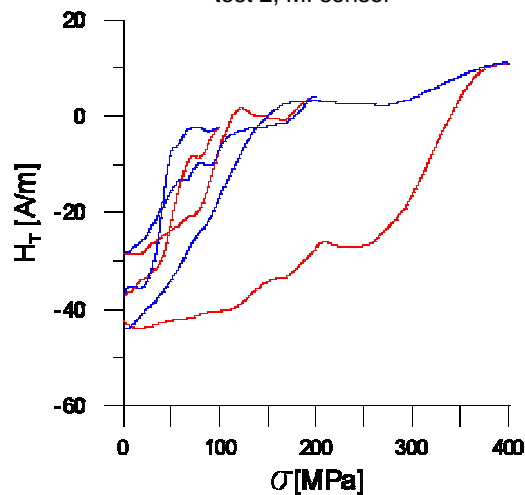


**Fig. 6a.** Magnetizing curves for a stabilized magneto-mechanical hysteresis loop sample 3 MI sensor

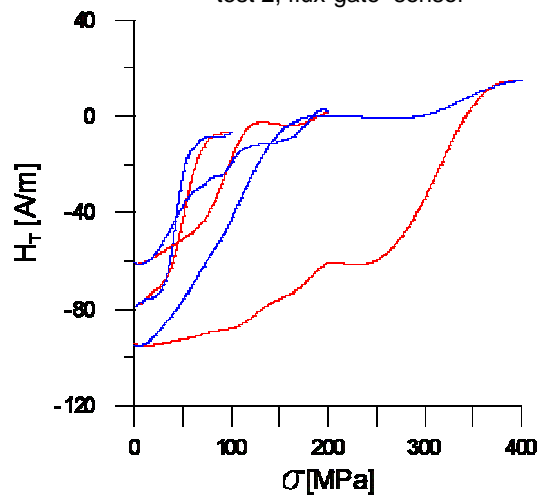


**Fig. 6b.** Magnetizing curves for a stabilized magneto-mechanical hysteresis loop sample 3, flux-gate sensor

As regards Figures 3 to 6, Fig 3a, 4a, 5a, 6a represent the results obtained for the magnetoimpedance sensor, and Figures 3b, 4b, 5b, 6b- for the flux-gate sensor. We can clearly observe similarity of the distribution patterns, with simultaneously large quantitative differences in the initial offset and amplification (about 2x) – attributable to different distances of magneto-sensitive elements of sensors and their spatial characteristics, as well as polarization of the sample by external magnetic field and stresses. This aspect appears thought-provoking, especially in the case of the quantitative use of values in diagnostic correlations.

Fig. 3a and 3b give the magnetization curves for the first three cycles at a maximum stress of 400 MPa and show that the greatest increase in RMF for sample 1 takes place in the first cycle of loading, and in each subsequent cycle the change decreases. This conclusion concerns mainly irreversible changes in magnetization, with relatively stable reversible changes. After stabilization of the magnetomechanical hysteresis loop, the subsequent changes of magnetization taking place as a result of changes in stress are practically only reversible changes.

The influence of the microstructure on magnetization patterns is readily apparent. The magnetization curve for sample 1 with a ferritic structure is different from that obtained for samples 2 and 3 where the martensitic is predominant. A summary of the maximum and minimum averages of the state of stabilized magneto-mechanical hysteresis is included in Table 3, the standard deviation “s” was also calculated.

**Table 3.** Summary of maximum and minimum values RMF

Sample no.	The value of the maximum stress	MI sensor				Flux-gate sensor			
		Maximum		Minimum		Maximum		Minimum	
		H <sub>s</sub> [A/m]	s	H <sub>s</sub> [A/m]	s	H <sub>s</sub> [A/m]	s	H <sub>s</sub> [A/m]	s
	0 MPa	-75,4		-83,21		-161,03		-172,52	
1	100 MPa	-72,44	0,87	-76,06	0,61	-152,50	0,56	-159,07	0,40
	200 MPa	-63,18	1,68	-74,43	0,79	-125,73	2,74	-150,75	0,92
	400 MPa	-36,59	0,53	-59,38	1,59	-73,69	1,43	-150,97	1,04
	Δ <sub>400-100</sub>	35,85		16,68		78,81		8,1	
2	0 MPa	-12,66		-55,42		-20,31		-92,18	
	100 MPa	-7,33	7,89	-35,78	2,53	-20,63	14,22	-77,74	7,23
	200 MPa	2,54	3,12	-39,40	6,68	-3,40	15,81	-84,20	14,92
	400 MPa	5,02	2,59	-43,40	7,92	3,71	5,74	-95,34	18,15
	Δ <sub>400-100</sub>	12,35		-7,62		24,34		-17,6	
3	0 MPa	-7,62		-39,4		-17,43		-85,4	
	100 MPa	-2,82	2,17	-44,51	7,84	-6,44	0,89	-78,36	0,89
	200 MPa	5,46	1,00	-27,41	0,89	4,15	1,35	-60,57	0,66
	400 MPa	9,96	0,68	-44,65	1,29	14,69	0,96	-95,81	2,31
	Δ <sub>400-100</sub>	12,78		-0,14		21,13		-17,45	
s - standard deviation, 0 MPa - approximate value after gripping jaws; Δ400-100 - difference in magnetic field component at 400 MPa and 100 MPa specimen load									

Figures 4 to 6 and Table 3 show that each combination of parameters - microstructure, maximum value of stress, corresponds to the characteristic variability pattern of magnetization and its maximum and minimum values. An increase in the cycle amplitude results in an increase in the maximum values obtained in the series, with the highest increase occurring for sample 1 with a ferritic structure. It was found that regardless of the amplitude



of the cycle, the highest values of maxima are registered for sample 3 (martensitic structure) and the smallest- for sample 1 (ferritic structure).

During an active experiment (on a material with a known strength and microstructure) observed changes in the tangent component of  $H_T$  field strength near the sample surface and the surface of the hysteresis loop of this component:

- do not provide unambiguous information about changes in the magnetic permeability of the sample material;
- influence of demagnetisation coefficient on the distribution of magnetic field near the sample.

This is a weakness of simplified measurements, which allow only fast detection of magnetic anomalies during a passive experiment. In order to quantitatively analyze changes in the microstructure during a passive experiment, it is necessary to measure 3 components of the magnetic field. Fig. 7 shows exemplary readouts from a triaxial magnetometer. The triaxial magnetometer provides new diagnostic features, including:

- amplitude of the magnetic field vector
- angle of deviation of the tangent vector component from the axis of the specimen
- the angle of inclination of the vector to the surface of the sample.

The analysis of the above parameters goes beyond the scope of this article.

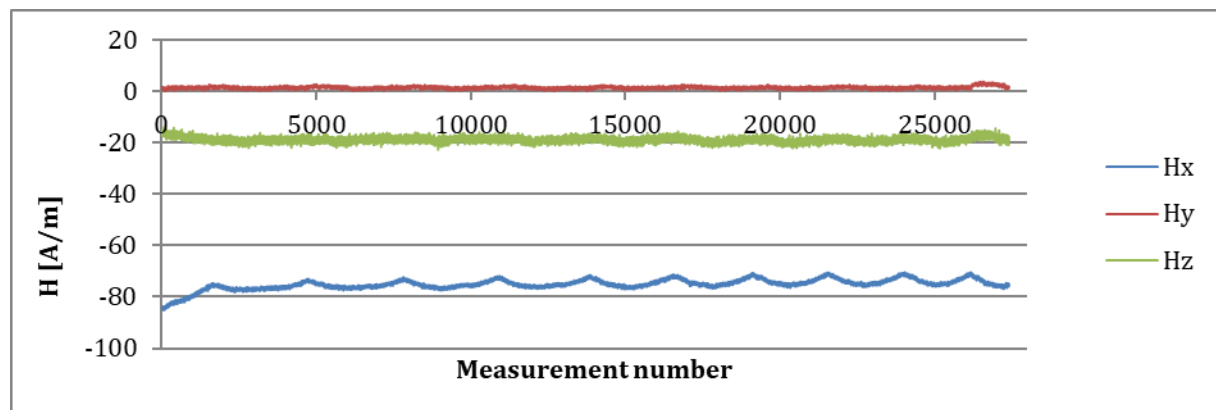


**Fig. 7.** Example of measurement with a triaxial sensor

## SUMMARY

Measurements of the residual magnetic field of diffusion (tangential component parallel to the load direction) were taken close (about 3 mm) to the surface of plate steel samples P91 (X10CrMoVNb9-1) subjected to periodic tensile pulsating cyclic loads. The tests program included a qualitative and quantitative comparison of readouts from various types of sensors (flux-gate and magnetoimpedance) and the analysis of the influence of microstructure and the maximum cycle stress on RMF values.

The influence of the microstructure on the variability pattern of the magnetization is clearly apparent. The magnetization curve for the ferritic structure differs significantly from that obtained for the martensitic structure.

Each combination of parameters - microstructure, maximum value of stress, corresponds to the characteristic variability pattern of magnetization and its maximum and minimum values. The increase in cycle amplitude causes the increase of the maximum values obtained in the series, with the highest increase registered for the ferritic structure. It was found that regardless of the amplitude of the cycle, the highest values of maxima are registered for sample 3 (martensitic structure) and the smallest- for sample 1 (ferritic structure).

## REFERENCES

1. Roskosz M., Metal magnetic memory testing of welded joints of ferritic and austenitic steels, *NDT&E International*, 44 (2011) 305–310, doi:10.1016/j.ndteint.2011.01.008
2. Roskosz M., Bieniek M., Evaluation of residual stress in ferromagnetic steels based on residual magnetic field measurements *NDT&E International*, 45 (2012) 55–62, doi:10.1016/j.ndteint.2011.09.007
3. Kwaśniewski J., Roskosz M., Witoś M., Molski Sz., Applications of magnetometric sensors based on amorphous materials in diagnostics of wire ropes. *Archives of Mining Sciences*, 63 (1) (2018), 221–227.
4. Kwaśniewski J., Application of the wavelet analysis to inspection of compact ropes using a high-efficiency device. *Archives of Mining Sciences*, 58(1) (2013), 159–164.
5. Sheng Bao, Meili Fu, Huangjie Lou, Shuzhuang Bai: Defect identification in ferromagnetic steel based on residual magnetic field measurements. *Journal of Magnetism and Magnetic Materials* 441 (2017), 590–597.
6. Juwei Zhang, Xiaojiang Tan, Pengbo Zheng: Non-Destructive Detection of Wire Rope Discontinuities from Residual Magnetic Field Images Using the Hilbert-Huang Transform and Compressed Sensing. *Sensors*, 17 (2017), 608; doi:10.3390/s17030608
7. Stegemann R., Cabeza S., Lyamkina V., Bruno G., Pittner A., Wimpory R., Boin M., Kreutzbruck M., Residual stress characterization of steel TIG welds by neutron diffraction and by residual magnetic stray field mappings. *Journal of Magnetism and Magnetic Materials* 426 (2017) 580–587.
8. Haihong Huang and Zhengchun Qian, Effect of Temperature and Stress on Residual Magnetic Signals in Ferromagnetic Structural Steel. *IEEE Transactions On Magnetics*, 53(1) (2017).
9. Haihong Huang, Zhengchun Qian, Cheng Yang, Gang Han, Zhifeng Liu, Magnetic memory signals of ferromagnetic weldment induced by dynamic bending load. *Nondestructive Testing and Evaluation*, 32(2), 166-184, DOI: 10.1080/10589759.2016.1159307
10. Haihong Huang, Gang Han, Zhengchun Qian, Zhifeng Liu, Characterizing the magnetic memory signals on the surface of plasma transferred arc cladding coating under fatigue loads. *Journal of Magnetism and Magnetic Materials*, 443 (2017), 281–286.
11. Venkatachalapathi N., Jameelbasha S.M.D, Janardhan Raju G., Raghavulu P., Characterization of Fatigued Steel States with Metal Magnetic Memory Method. *Materials Today, Proceedings* 5 (2018) 8645–8654.

12. Jiles D. C., Atherton D. L., Theory of ferromagnetic hysteresis, J. Magn. Magn. Mater., 61 (1986), 48–61.
13. Jiles D. C., Introduction to Magnetism and Magnetic Materials. London: Chapman and Hall, 1991.
14. Jiles D. C., Theory of the Magnetomechanical Effect, J. Phys. D: Appl. Phys., 28 (1995) 1537–1546.
15. <https://www.tiniusolsen.com/>
16. <https://www.ptsndt.com>
17. <http://www.energodiagnostika.com/Default.html>
18. [http://www.micromagnetics.com/product\\_page\\_spi\\_nmeter3.html](http://www.micromagnetics.com/product_page_spi_nmeter3.html)
19. <https://ngdc.noaa.gov/geomag/WMM/DoDWMM.shtml>